IOP PUBLISHING NANOTECHNOLOGY
Nanotechnology 23 (2012) 495604 (10pp) doi:10.1088/0957-4484/23/49/495604

Altering the dewetting characteristics of ultrathin gold and silver films using a sacrificial antimony layer

P Farzinpour, A Sundar, K D Gilroy, Z E Eskin, R A Hughes and S Neretina

College of Engineering, Temple University, Philadelphia, PA 19122, USA

E-mail: hughesr@temple.edu and neretina@temple.edu

Received 23 August 2012, in final form 23 October 2012
Published 16 November 2012
Online at stacks.iop.org/Nano/23/495604

Abstract

Solid state dewetting of ultrathin films is the most straightforward means of fabricating substrate-supported noble metal nanostructures. This assembly process is, however, quite inflexible, yielding either densely packed smaller structures or widely spaced larger structures. Here, we demonstrate the utility of introducing a sacrificial antimony layer between the substrate and noble metal overlayer. We observe an agglomeration process which is radically altered by the concurrent sublimation of antimony. In stark contrast with conventional dewetting, where the thickness of the deposited metal film determines the characteristic length scales of the assembly process, it is the thickness of the sacrificial antimony layer which dictates both the nanoparticle size and interparticle spacing. The result is a far more flexible self-assembly process where the nanoparticle size and areal density can be varied widely. Demonstrations show nanoparticle areal densities which are varied over four orders of magnitude assembled from the identical gold layer thickness, where the accompanying changes to nanostructure size see a systematic shift in the wavelength of the localized surface plasmon resonance. As a pliable self-assembly process, it offers the opportunity to tailor the properties of an ensemble of nanostructures to meet the needs of specific applications.

S Online supplementary data available from stacks.iop.org/Nano/23/495604/mmedia

(Some figures may appear in colour only in the online journal)

1. Introduction

Precious metal nanostructures immobilized on substrate surfaces are of importance for numerous potential applications in the areas of photovoltaics [1], catalysis [2], chemical and biological sensing [3], the formation of nanowires via the vapor–liquid–solid growth mode [4] and as shadow masks for reactive ion etching [5]. Early stage investigations in these emerging fields often relied heavily on substrate-based nanostructures derived from the room temperature deposition of continuous ultrathin films onto substrates followed by their subsequent agglomeration at elevated temperatures [6–9]. The widespread use of this thermal solid state dewetting process, however, was largely reliant on the ease with which such nanostructures can be fabricated over large areas, typically produced in a few hours using simple instrumentation consisting of a room temperature sputter coater and a tube furnace. Apart from this simplicity aspect, the nanostructures produced were unsatisfactory from many standpoints as there was a lack of control over the nanoparticle size distribution, spacing and placement on the substrate. As technologies mature the specifications placed on the nanomaterials grow increasingly stringent as efforts focus on tailoring the collective response derived from an ensemble of nanostructures to meet the requirements of a particular application. As a result, the use of the dewetting phenomenon has often been marginalized in favor of more sophisticated and often more costly approaches [1–4].

The dewetting phenomenon is driven by an interplay between thermodynamics and kinetics. While thermodynam-

ics always drives the system toward the most energetically favorable state, atom kinetics often prevent this state from being reached. This is a simple consequence of the fact that atoms often encounter energy barriers which they have insufficient kinetic energy to overcome, a circumstance which confines the system to a metastable state. A continuous ultrathin metal film deposited on a substrate at room temperature exists in such a metastable state if the surface energy of the metal is greater than that of the substrate material. Thermodynamics drives such a system toward a geometry which will reduce the surface area of the metal. This geometry, however, is unattainable because the metal atoms lack the kinetic energy required to move significant distances across the surface. The end result is a continuous metastable film. Heating such a film drives it toward the equilibrium state, which sees it agglomerate into metal nanostructures at temperatures well below the melting point of the metal. This process, commonly referred to as solid state dewetting [10], is typically initiated at holes in the film which extend through the film to the substrate surface. Such holes typically originate at grain boundary triple junctions [10]. Agglomeration then proceeds through solid state surface diffusion away from the step edges. The overall process is quite complex with Rayleigh-like instabilities [11], fingering instabilities [12], grain boundaries [13] and substrate surface texture [11] all playing a decisive role. In general, thinner films dewet at lower temperatures, forming nanostructures which are smaller and more densely packed [14]. The nanostructures formed are usually well bonded to the substrate, having a contact angle determined by surface energy considerations, obeying Young's equation subjected to retention forces [15] for large particle sizes, but where this relationship is altered somewhat on the nanoscale [16]. The structures formed are also influenced by the crystallographic orientation of the substrate [17] and film [18], the lattice mismatch between the substrate and metal [17], substrate surface reconstructions [19], nanostructure faceting [20] and interface chemistry [21].

Numerous approaches have been devised to manipulate the dewetting phenomenon in an effort to control the placement of the dewetted metal structures as they agglomerate on the surface of a substrate. These so-called templated assembly techniques, which impose a periodicity onto the dewetting process through the use of lithographically defined film edges [14, 18, 22–24], periodic templates [14, 25, 26] or substrate surface texture [27–29], have proved highly successful in generating arrayed structures. They are, however, often limited in terms of the minimum size and/or areal density of structures achievable. In many cases they are also technically challenging and their cost is prohibitive. When non-arrayed structures are formed on polished substrates there are no such limitations, but there exists limited flexibility in terms of tuning the nanoparticle size distribution and interparticle spacing. The size distribution can be altered by maintaining the nanostructures at elevated temperatures. This induces Ostwald ripening, which is a disproportionate exchange of atoms between the nanostructures via substrate surface diffusion which favors larger structures at the expense of smaller ones [30, 31]. The step-terrace structures associated with vicinal surfaces have also been shown to alter both the nanostructure placement and size distribution [32]. It has also been shown that the nanoparticle size distribution can be narrowed through the placement of a metal foil on the free surface of the film as it dewets [33]. In this case, the larger nanoparticles contact the metal foil and sink atoms onto it, reducing their size while leaving the smaller nanostructures intact.

In a previous report, we demonstrated a processing route for the fabrication of nanostructured gold and silver arrays using a templated assembly technique referred to as dynamic templating [26]. The technique involved the formation of a periodic array of sacrificial antimony pedestals topped with an ultrathin layer of a precious metal. When heated, the antimony preferentially sublimates from the sides of the pedestal causing the areal dimensions of the pedestal, on which the precious metal is agglomerating, to rapidly shrink. This leads to a forced migration of the precious metal to the center of each pedestal, where the rate and areal extent over which the agglomeration occurs far exceed that of a precious metal pedestal deposited directly on the substrate surface. At the end of the process, the antimony has completely sublimed, leaving behind a periodic array of precious metal nanostructures. The density of the structures produced, however, is limited by the feature size of the shadow masks used. In this paper we detail the dewetting characteristics of continuous gold and silver films deposited on sacrificial layers of antimony, which are continuous. It is demonstrated that variations to both the thickness of the precious metal and the antimony layer allow for the manipulation of the size distribution, spacing and plasmonic properties of the nanoparticle ensemble, a result which allows one to tailor the nanoparticle properties to specific applications.

2. Sample preparation and characterization

Figure 1 shows a schematic of the procedure used to obtain substrate-supported gold nanoparticles. It begins with the deposition of a sacrificial antimony layer over which an ultrathin gold layer is deposited. Heating the layered structure results in the agglomeration of gold, but where its dewetting characteristics are strongly influenced by the concurrent sublimation of antimony. At the end of the process all the antimony has sublimed, leaving immobilized gold nanoparticles on the surface of the substrate. The experiments were carried out on (0001)-oriented Al_2O_3 substrates (i.e. *c*-plane sapphire). This surface is ideal for such studies due to its low surface energy, high chemical and thermal stability, crystallographic perfection and high resistance to gold and silver interdiffusion. The fact that this substrate is optically transparent also allows for the straightforward characterization of the plasmonic response. The dewetting characteristics of gold on sapphire in the absence of a sacrificial antimony layer were mapped out for film thicknesses ranging from 0.7 to 24 nm. Twenty-four samples were then used to characterize the influence of the antimony layer on the gold dewetting process. For this series

of samples, four gold film thicknesses of 0.7, 2, 4 and 8 nm were each deposited on antimony layers having thicknesses of 2.5, 5, 7.5, 10, 20 and 40 nm. For the silver dewetting experiments a film of thickness of 2 nm was deposited on a bare substrate and compared to silver deposited on antimony layers having thicknesses of 1.5, 3, 4.5 and 6 nm. All depositions were carried out in a Gatan High Resolution Ion Beam Coater using 99.9985% purity targets. The quoted film thicknesses are obtained using deposition rates derived from atomic force microscopy (AFM) measurements on the step-edges formed through the deposition of films through shadow masks. Films in groups of four, where each had the same antimony content, were placed in an alumina crucible and inserted into a tube furnace (Lindberg Blue M). Four quartz tubes dedicated to the dewetting of (i) gold, (ii) gold with antimony, (iii) silver and (iv) silver with antimony were used in order to prevent cross-contamination. All experiments were carried under a 100 sccm flow of ultra-high purity argon where the tube was thoroughly flushed with argon prior to heating. All gold samples used a heating regimen which sees the sample ramped to 900 °C in 45 min where it is held for 15 min, after which it is allowed to cool to room temperature over the course of a few hours. Samples were then cycled to high temperatures a second time, a procedure which proved effective in ridding the sample of trace amounts of antimony. It is noted that the four samples having no antimony were also temperature cycled in order to obtain fair comparisons. Silver dewetting experiments were also carried out in a similar manner, but where the samples were heated to 750 °C in 30 min. The lower temperature prevented significant silver evaporation. The plasmonic properties of all samples were characterized using a JASCO V530 UV/VIS spectrophotometer. Scanning electron microscopy (SEM) images, obtained using either an FEI Quanta 400 or 600 FEG ESEM and processed using ImageJ software [34], were used to obtain distributions of the nanoparticle size and spacing.

3. Results

Figure 2(a) shows SEM images of nanostructures derived from gold films of various thicknesses which have dewetted on sapphire substrates. Such images were used to extract the dependency of the nanoparticle areal density (figure 2(b)), the nanoparticle diameter (figure 2(c)) and the interparticle spacing (figure 2(d)) on the initial gold film thickness. Nanoparticle diameters and interparticle spacings were extracted from distributions where the plotted value is the histogram maximum. The interparticle spacing measurements correspond to the center-to-center nearest-neighbor distances. The overall dewetting behavior observed is consistent with previous studies [13, 14] and provides baseline parameters characteristic of the conventional dewetting process. As the gold film thickness is increased from 0.7 to 24 nm there is a nearly four orders of magnitude decrease in the density of nanoparticles which is accompanied by a continuous rise in both the nanoparticle diameter and the interparticle distance. The overall process is thus characterized by agglomeration which occurs on increasingly larger length scales as the

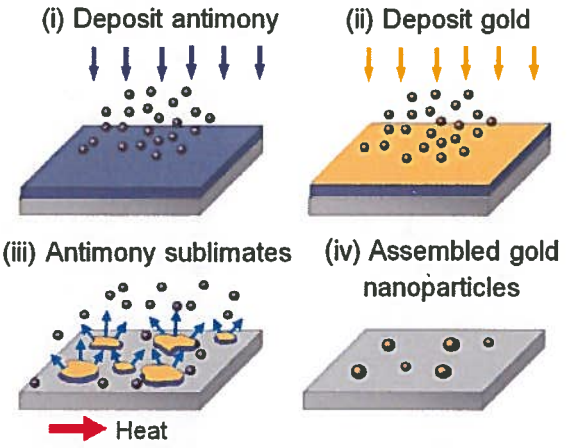

Figure 1. Schematic of the procedure used to fabricate substrate-supported gold nanoparticles. The process proceeds by (i) depositing a sacrificial antimony layer followed by (ii) the deposition of an ultrathin gold film. (iii) The sample is then heated to high temperatures to simultaneously induce the dewetting of gold and the sublimation of antimony. At the end of the assembly process all of the antimony has sublimed leaving behind (iv) substrate-supported gold nanoparticles.

gold layer thickness is increased. The assembly process thus yields either densely packed smaller structures or widely spaced larger structures. It is noteworthy that for a given film–substrate combination little can be done in terms of processing conditions to significantly alter this behavior.

Figure 3(a) shows a matrix of SEM images which map out the influence that a sacrificial antimony layer has on the dewetting characteristics of ultrathin gold films. Each row in the matrix corresponds to the same antimony layer thickness while each column corresponds to the same gold thickness. For any individual antimony thickness (i.e. the rows of the matrix) the trend is for the nanoparticle size to increase as the thickness of the gold layer increases, a trend identical to that observed when gold films are deposited directly on a bare substrate. However, the usual trend toward decreasing nanoparticle density for thicker gold layers, while remaining intact for thin antimony layers, becomes increasingly corrupted as the layer thickness is increased. The trend observed as the antimony thickness is varied while holding the gold thickness constant (i.e. the columns of the matrix) is quite dramatic, showing a remarkable increase in both the nanoparticle size and interparticle spacing. These changes are accompanied by a nearly four orders of magnitude change in the nanoparticle density (figure 3(b)). It is also noted that the observed trends continue well outside the extent of the matrix shown, ultimately giving rise to particles of micrometer-scale diameter with interparticle spacings near 10 micrometers. This ability to radically alter the nanoparticle size, spacing and density while maintaining a constant gold film thickness has not previously been demonstrated. To further illustrate this point, figure 4 shows the SEM images, histograms of the nanoparticle diameter and interparticle spacing, and spectra of the extinction efficiency for 2 nm thick gold films dewetted on antimony layers of various

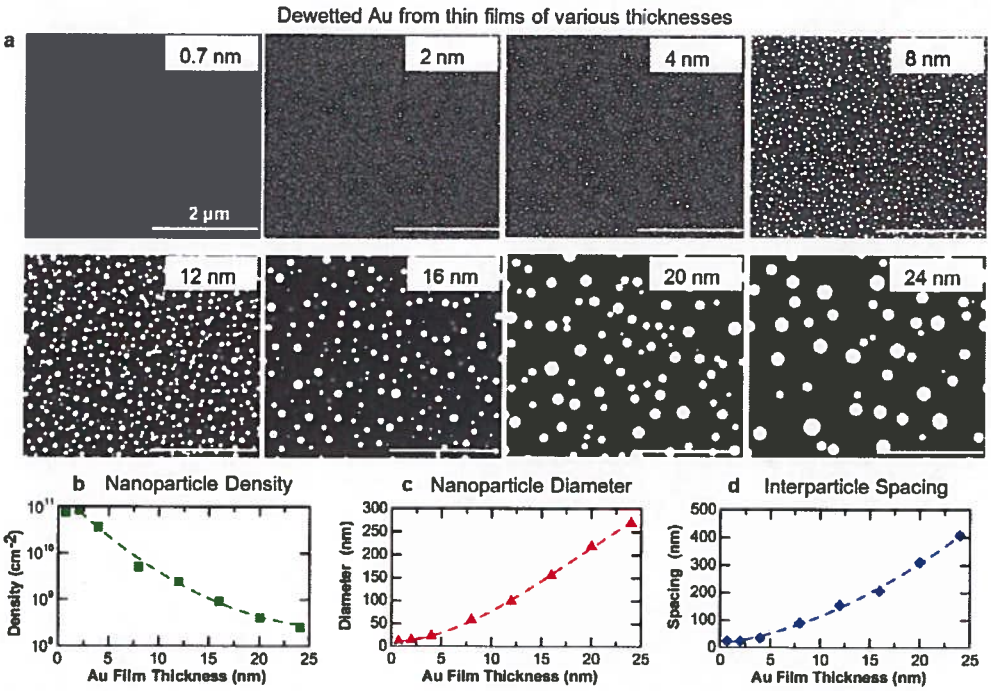

Figure 2. Summary of the solid state dewetting behavior for gold films deposited on (0001)-oriented sapphire substrates. (a) SEM images of gold nanoparticles obtained through the dewetting of continuous films for thicknesses ranging from 0.7 to 24 nm (scale bar = 2 μm). Extracted from the images are the dependences of the nanoparticle areal density (b), diameter (c) and interparticle spacing (d) on the gold film thickness. The lines drawn through the data points are a guide for the eye.

thicknesses. A systematic shift in the distributions from smaller to larger nanoparticle diameters and from closely to sparsely spaced nanoparticles is evident as the thickness of the sacrificial antimony layer is increased. As expected, the extinction efficiency shows a corresponding red-shift in the wavelength of the localized surface plasmon resonance (LSPR) resulting from the larger nanoparticles assembled. The complete dataset, showing histograms, the extinction spectra and a statistical analysis for all samples shown in figure 3 is included as supporting information (figures S1–S3, tables S1 and S2 available at stacks.iop.org/Nano/23/495604/mmedia).

Silver nanoparticles were also assembled on sapphire substrates using a sacrificial antimony layer. Figure 5 shows the SEM images, histograms of the nanoparticle diameter and interparticle spacing, and spectra of the extinction efficiency for 2 nm thick silver films dewetted on antimony layers of various thicknesses. In a manner quite similar to gold nanoparticle assembly, there exists a systematic increase in the nanoparticle diameter and interparticle spacing as well as a red-shift in the LSPR peak position as the antimony layer thickness is increased. There are, however, a number of key differences. Foremost is the larger characteristic length scale over which silver agglomerates compared to gold. There also exists a discontinuity in the trends for nanoparticle size and interparticle spacing as the thickness of the antimony layer transitions from 3 to 4.5 nm. The silver nanoparticles also show a stronger tendency to facet.

4. Discussion

The results presented demonstrate that the introduction of a sacrificial antimony layer results in an assembly process which is far more flexible. In contrast with conventional dewetting, where the characteristic length scales of the assembly process are driven by the thickness of the gold film, the nanoparticle size and interparticle spacing are largely determined by the thickness of the sacrificial antimony layer. The end result is a self-assembly process where the gold layer thickness determines the quantity of gold to be agglomerated, while the antimony layer thickness dictates the characteristic length scale over which the agglomeration occurs. This distinction allows for a pliable assembly process where the nanoparticle size and areal density can be varied independently, the result of which is a process yielding substrate surfaces supporting gold nanostructures with characteristic length scales unattainable via the conventional route. The incorporation of a sacrificial antimony layer into the assembly process also has its shortcomings. Most notable is the trend toward increasing widths in the nanoparticle size distributions as both the gold and antimony layer thickness is increased. For such samples the assembly process gives rise to large nanoparticles containing most of the gold initially deposited, but which are surrounded by numerous smaller nanoparticles. This deficiency is most acute for the gold nanoparticles assembled from the 8 nm gold film deposited on a 10 nm sacrificial antimony layer, where 50% of the nanoparticles account

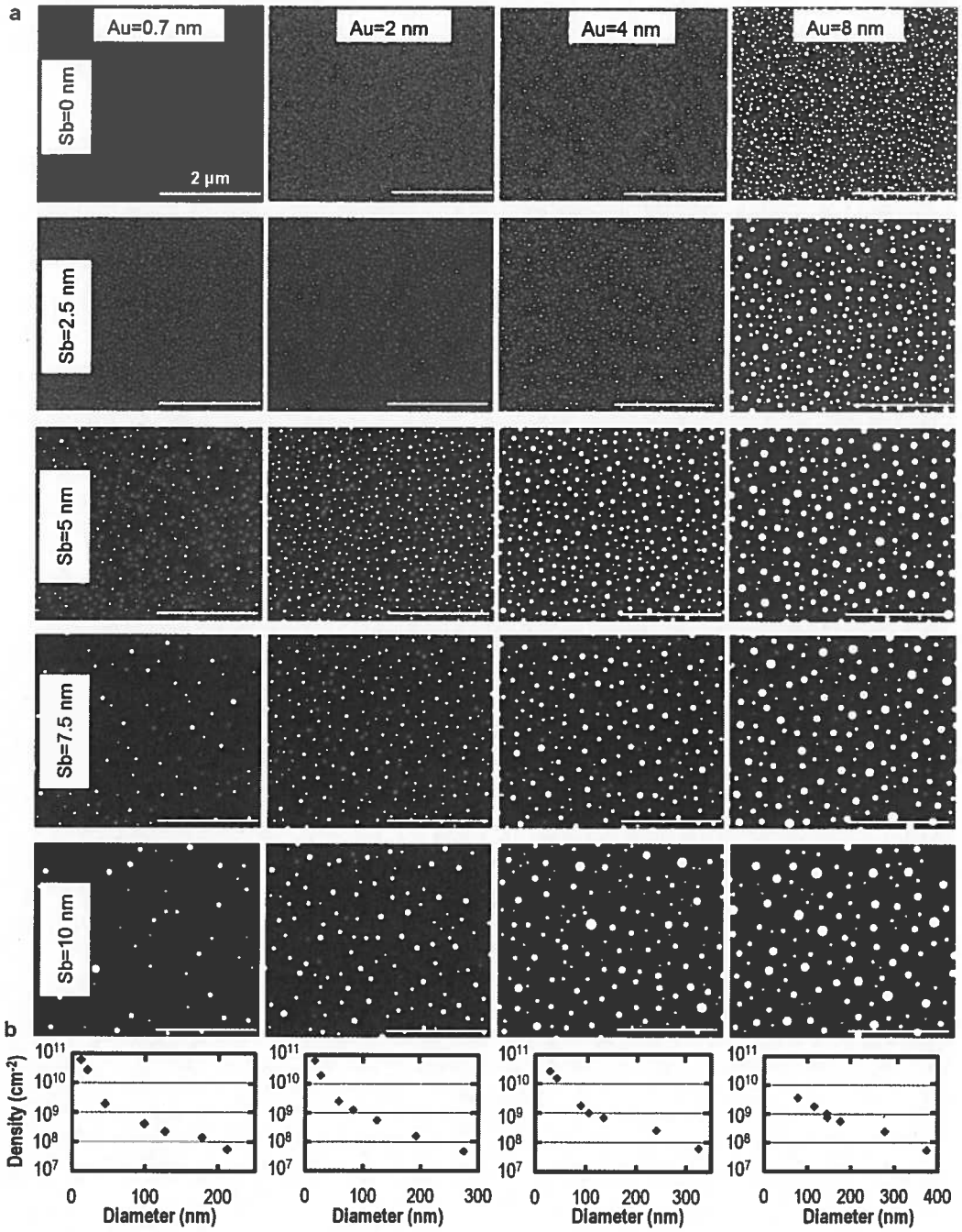

Figure 3. Summary of the dewetting behavior for gold films deposited on a sacrificial antimony layer. (a) A matrix of SEM images of gold nanoparticles obtained through the dewetting of continuous films of gold deposited on sacrificial antimony layers. For each image the gold film thickness used is at the top of the column and the antimony thickness is to the left of each row (scale bar = 2 μm). (b) Corresponding plots of the nanoparticle density versus the average nanoparticle diameter for each gold film thickness. For each plot the seven data points shown correspond to antimony thicknesses of 0, 2.5, 5, 7.5, 10, 20 and 40 nm (left to right). Excluded from these density calculations are the smallest nanoparticles (3% by volume) as they tend to distort the overall trend.

for only 10% of the nanoparticle volume (supporting information, figure S1 available at stacks.iop.org/Nano/23/495604/mmedia). With so many low volume nanoparticles, Ostwald ripening and/or evaporation [35] provides an obvious avenue for significantly narrowing the size distribution; this was not pursued in this comparative study so as to maintain consistency in the processing conditions.

The overall role the sacrificial layer plays is to enhance the areal extent over which the dewetting occurs, where control is attained through adjustments to the layer thickness.

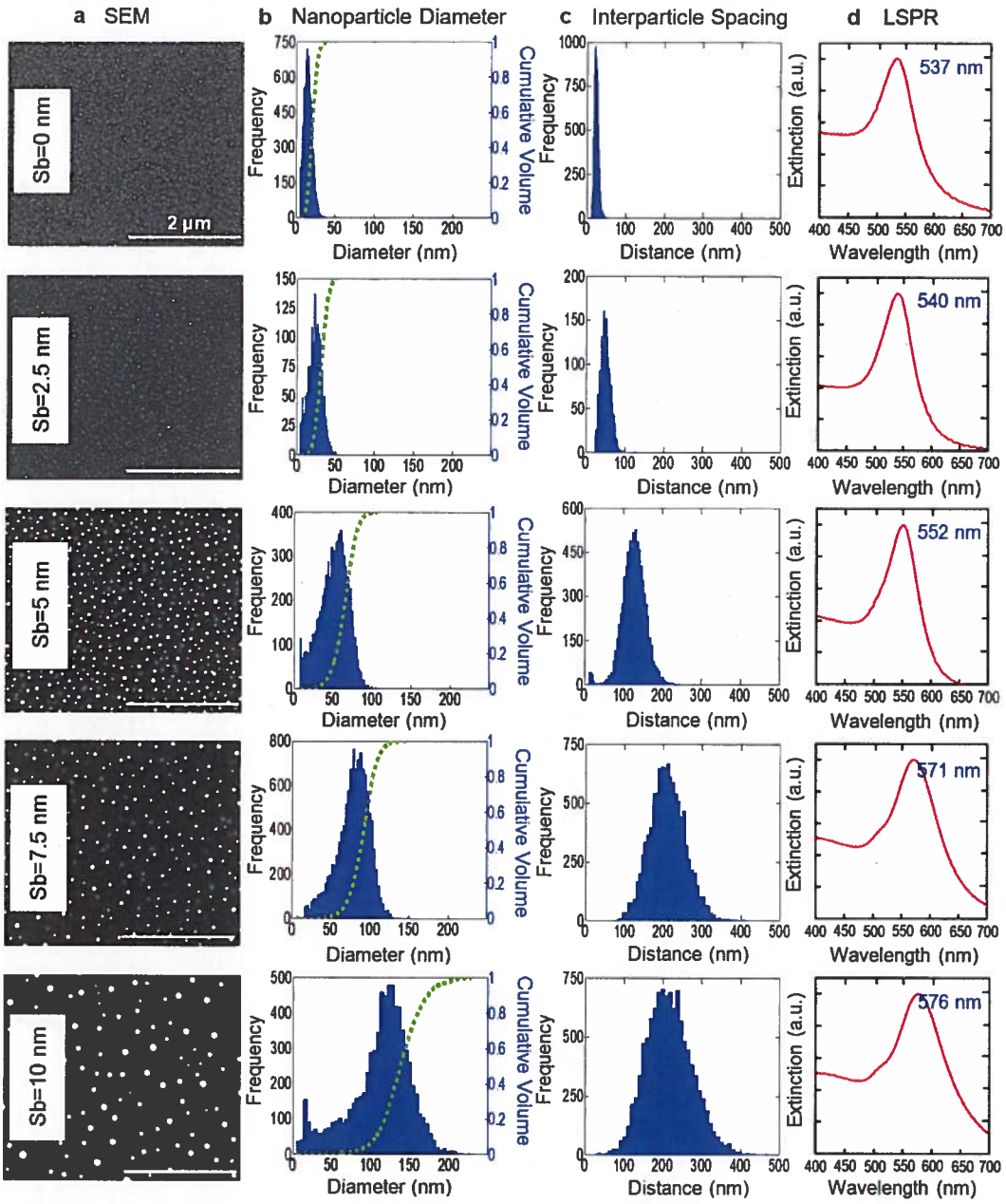

Figure 4. Summary of the dewetting behavior for 2 nm thick gold films deposited on sacrificial antimony layers with thicknesses of 0, 2.5, 5, 7.5 and 10 nm. Note that systematic variations corresponding to the antimony layer thickness used are observed in (a) the SEM images of the gold nanoparticles (scale bar = 2 μm), (b) the histograms of the nanoparticle size distribution, (c) the histograms of the interparticle spacing and (d) the LSPR peak position. Frequency refers to the number of times a particular diameter (b) or distance (c) has been observed in the SEM images analyzed. Overlaid over each of the nanoparticle diameter histograms (b) is a normalized plot of the cumulative nanoparticle volume for all the histogram bins to the left of the curve. The vast majority of gold atoms can thus be found in nanoparticles having dimensions which correspond to the rapid rise in the curve.

The effectiveness of antimony as the sacrificial layer stems from a set of rather unique properties associated with both it and the combined gold–antimony binary system. Antimony readily sublimates at temperatures where the gold assembly occurs. It has a surface energy well below that of most common metals [36], a property which makes it more prone to the wetting of surfaces. In the solid state it is nearly immiscible with gold (miscibility 0.75 wt% Sb). This immiscibility results in the inhibition of antimony sublimation when coated with a gold layer [26] as the incompatibility of these two elements imposes a barrier to a process which would otherwise see the interdiffusion of antimony through

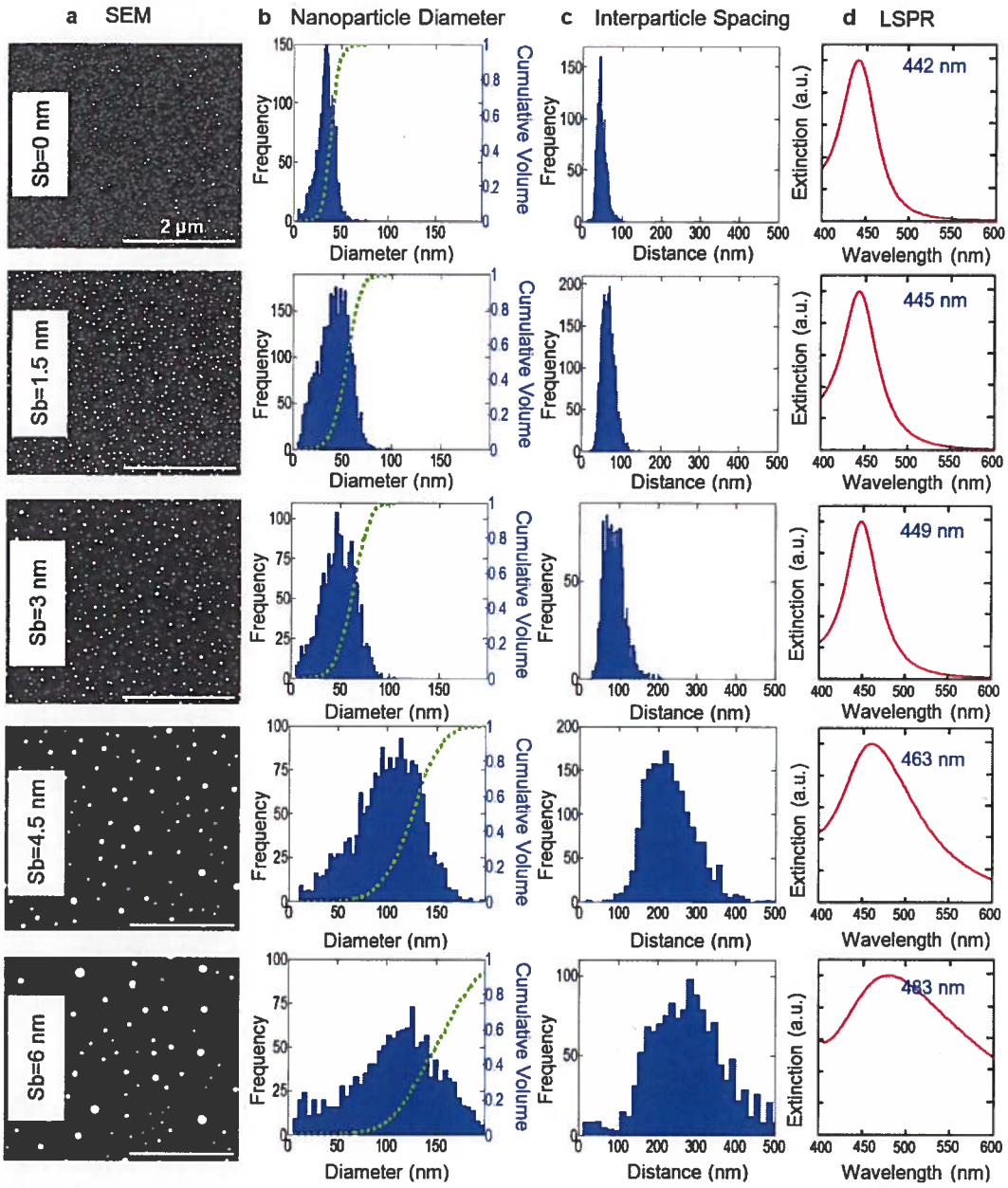

Figure 5. Summary of the dewetting behavior for 2 nm thick silver films deposited on sacrificial antimony layers with thicknesses of 0, 1.5, 3, 4.5 and 6 nm. Note that the (a) SEM images of the silver nanoparticles (scale bar = 2 μm), (b) histograms of the nanoparticle size distribution, (c) histograms of the interparticle spacing and (d) extinction efficiency spectra all show trends similar to that observed for gold.

the gold overlayer followed by its subsequent release from the surface. At sufficiently elevated temperatures, however, immiscibility gives way to miscibility as antimony and gold intermix, forming a low temperature eutectic ($T_E = 360\,°C$). The silver–antimony binary system shares many of these same features, but where both the eutectic temperature ($T_E = 485\,°C$) and antimony miscibility in silver (miscibility 8 wt% Sb) are significantly higher.

The mechanisms guiding the enhancements to the areal extent over which the gold agglomeration occurs have been discussed previously within the context of the templated assembly of ultrathin gold layers deposited atop antimony pedestals [26]. For this scenario, it was observed that the gold layer inhibits antimony sublimation from the pedestal top. Antimony sublimation from its sides, however, is uninhibited. It is the resulting advancement of the sublimation fronts from all sides toward the center of the pedestal which rapidly drives the agglomeration of gold to a single location as the antimony supply is steadily reduced to the point of exhaustion. Also crucial to the assembly process is the simultaneous dissolution

of antimony into the gold overlayer, a process which induces a reactive wetting process and leads to the formation of a gold–antimony eutectic at the interface. Our expectation is that the assembly processes observed in the current study proceeds in much the same manner as for the templated case. Key differences, however, arise from: (i) the fact that the gold film must rupture in order to generate the antimony sublimation fronts required to initiate the assembly process and (ii) the antimony–gold ratio is much lower than that used in the previous study. The initiation of the dewetting process by rupturing the film is not unique to the assembly process studied here. In fact, conventional solid state dewetting is reliant on the formation of voids at grain boundary defects which extend from the surface of the film to the underlying substrate from which atoms retreat. *In situ* monitoring of this conventional dewetting process [13] reveals that the entire film dewets from these voids through a repetitive process which sees the edge thicken, become unstable due to Rayleigh-like instabilities, shed material to form isolated islands and then thicken again. While similar monitoring will be required to delineate the exact processes by which films agglomerate in the presence of a sacrificial antimony layer, a number of factors relevant to the assembly process can, at this point, be articulated.

The interface between the noble metal and sacrificial antimony layer, over the course of the assembly process, evolves from one formed between two nearly immiscible solid state components to one which is a liquid eutectic [26]. While the propagation of the sublimation front drives the agglomeration process, the mere presence of the interface in the absence of this front favors kinetic processes which tend to maintain a continuous film on its surface. Studies of the antimony–silver interface, for example, demonstrate the effectiveness of antimony as a kinetically active surface agent (i.e. surfactant mediated epitaxy [37, 38]) able to transform the silver thin film growth mode from one which sees islands form and merge (i.e. the Volmer–Weber mode) to one where a single continuous layer forms before the growth of the next layer is initiated (i.e. the Frank–van der Merwe mode) [39, 40]. It is noteworthy that both experiment and calculations based on density-functional theory [41] show that the presence of antimony promotes the formation of smooth silver films while maintaining an interface which remains segregated. Such behavior is likely to be in opposition to the agglomeration of silver while on the surface of antimony. It would not be unexpected if the gold–antimony interface behaved similarly. Also in opposition to agglomeration processes is the kinetics associated with the formation of the eutectic. As antimony dissolves into the noble metal overlayer, the resulting dissolution is likely to promote non-equilibrium reactive wetting [42–44] which will also tend toward maintaining a continuous layer. Such tendencies toward maintaining film continuity are likely to play a pivotal role in increasing the characteristic length scale over which the film ultimately agglomerates by limiting the number of locations where the film ruptures. In terms of maintaining the film continuity, thicker noble metal layers are expected to be more robust and, as a result, rupture in fewer locations. Once the sublimation front arrives it will override all of these wetting tendencies, activating the agglomeration process and cutting off the supply of antimony upon which these tendencies are reliant.

Attempts to use antimony pedestals to promote the templated assembly of a wide variety of elements revealed that the formation of a eutectic at the interface was crucial in promoting agglomeration over large length scales [26]. Antimony was relatively ineffective in promoting the agglomeration of elements for which it does not share a low temperature eutectic. This limitation, however, was overcome through the introduction of a thin bismuth layer at the interface which becomes liquid during the assembly process. With the need to maintain a liquid interface, it is not unexpected that the antimony–gold ratio is critically important for the assembly process described in the present paper. Results indicate that as long as there remains an ample supply of antimony the gold assembly seems relatively unencumbered over large length scales. It, therefore, follows that the assembly mechanism is inhibited when utilizing a low antimony–gold ratio due to a lack of antimony. In this regime, the sublimation fronts will locally decrease the relative antimony-to-gold ratio as it drives gold forward and exhausts the antimony supply through sublimation. Both of these factors will eventually drive the system from the liquid to the solid phase field of the binary phase diagram. Should this occur, the motion of the advancing front will be impeded, taking on a character more akin to conventional solid state dewetting which will shed material in the form of isolated islands due to Rayleigh-like instabilities. After the material is shed, however, a new sublimation front will emerge and the process will be repeated. The fact that the SEM images consistently show parallel lines and concentric arcs of nanostructures, provide evidence for the existence of these propagating fronts and also indicate that they are large compared to the interparticle spacing. When thicker antimony layers are used, but where the gold thickness is held constant, the sublimation front will propagate further before shedding material, yielding larger nanostructures in the process. If the break between the island structures and the new sublimation front is disorderly, it could spawn the formation of many small antimony islands containing small quantities of gold. The subsequent assembly of these structures would account for the high number of smaller nanostructures observed when both the noble metal and antimony layer thicknesses are large.

5. Summary

In summary, we have devised a pathway for the assembly of noble metal nanostructures utilizing the dewetting phenomenon which allows for control over the nanostructure size and interparticle spacing. By merely varying the thickness of a sacrificial antimony layer placed between the substrate surface and the overlying metal film, it is now possible to dictate the characteristic length scales over which the agglomeration occurs. For a given metal thickness a thicker sacrificial layer will give rise to larger structures of low density, while a thinner layer gives rise to a high density of

smaller structures. The assembly route allows one to tailor the nanoparticle size and spacing to meet the needs of specific applications. As solar cell enhancement agents [1], seeds for the catalytic growth of nanowires [4] and as nanoscale masks for reactive ion etching [5], the resulting ensembles of noble metal nanostructures could prove particularly attractive.

Acknowledgments

This work is partially funded by the NSF CAREER award to SN (DMR-1053416). The authors acknowledge the expertise of Dr Frederick Monson (Technical Director, Center for Microanalysis, Imaging, Research and Training, West Chester University) and Dr G Baran for providing access to the AFM. KDG and ZEE acknowledge support received through a Temple University Graduate Student Fellowship and an NSF NUE Award (EEC-1042071), respectively.

References

[1] Atwater H A and Polman A 2010 Plasmonics for improved photovoltaic devices *Nature Mater.* **9** 205–13
[2] Ma Z and Dai S 2011 Development of novel supported gold catalysts: a materials perspective *Nano Res.* **4** 3–32
[3] Jans H and Huo Q 2012 Gold nanoparticle-enabled biological and chemical detection and analysis *Chem. Soc. Rev.* **41** 2849–66
[4] Dick K A 2008 A review of nanowire growth promoted by alloys and non-alloying elements with emphasis on Au-assisted III–V nanowires *Prog. Cryst. Growth Charact.* **54** 138–73
[5] Strobel S, Kirkendall C, Chang J B and Berggren K K 2010 Sub-10 nm structures on silicon by thermal dewetting of platinum *Nanotechnology* **21** 505301
[6] Pillai S, Catchpole K R, Trupke T and Green M A 2007 Surface plasmon enhanced silicon solar cells *J. Appl. Phys.* **101** 093105
[7] Valden M, Lai X and Goodman D W 1998 Onset of catalytic activity of gold clusters on titania with the appearance of nonmetallic properties *Science* **281** 1647–50
[8] Van Duyne R P, Hulteen J C and Treichel D A 1993 Atomic force microscopy and surface-enhanced Raman spectroscopy. I. Ag island films and Ag film over polymer nanosphere surfaces supported on glass *J. Chem. Phys.* **99** 2101–15
[9] Hiruma K, Yazawa M, Katsuyama T, Ogawa K, Haraguchi K, Koguchi M and Kakibayashi H 1995 Growth and optical-properties of nanometer-scale GaAs and InAs whiskers *J. Appl. Phys.* **77** 447–62
[10] Thompson C V 2012 Solid-state dewetting of thin films *Annu. Rev. Mater. Res.* **42** 399–434
[11] Giermann A L and Thompson C V 2005 Solid-state dewetting for ordered arrays of crystallographically oriented metal particles *Appl. Phys. Lett.* **86** 121903
[12] Kan W and Wong H 2005 Fingering instability of a retracting solid film edge *J. Appl. Phys.* **97** 043515
[13] Jiran E and Thompson C V 1992 Capillary instabilities in thin, continuous films *Thin Solid Films* **208** 23–8
[14] Müller C M, Mornaghini F C F and Spolenak R 2008 Ordered arrays of faceted gold nanoparticles obtained by dewetting and nanosphere lithography *Nanotechnology* **19** 485306
[15] Tadmor R, Bahadur P, Leh A, N'guessan H E, Jaini R and Dang L 2009 Measurement of lateral adhesion forces at the interface between a liquid drop and a substrate *Phys. Rev. Lett.* **103** 266101
[16] Liu F 2002 Self-assembly of three-dimensional metal islands: nonstrained versus strained islands *Phys. Rev. Lett.* **89** 246105
[17] Devenyi G A, Li J F, Hughes R A, Shi A C, Mascher P and Preston J S 2009 Epitaxially driven formation of intricate supported gold nanostructures on a lattice-matched oxide substrate *Nano Lett.* **9** 4258–63
[18] Ye J and Thompson C V 2011 Templated solid-state dewetting to controllably produce complex patterns *Adv. Mater.* **23** 1567–71
[19] Silly F and Castell M R 2005 Selecting the shape of supported metal nanocrystals: Pd huts, hexagons, or pyramids on $SrTiO_3$(001) *Phys. Rev. Lett.* **4** 046103
[20] Curiotto S, Chien H, Meltsman H, Wynblatt P, Rohrer G S, Kaplam W D and Chatain D 2011 Orientation relationships of copper crystals on *c*-plane sapphire *Acta Mater.* **59** 5320–31
[21] Hajjar S *et al* 2011 Morphology and composition of Au catalysts on Ge(111) obtained by thermal dewetting *Phys. Rev.* B **84** 125325
[22] Lee F Y, Fung K H, Tang T L, Tam W Y and Chan C T 2009 Fabrication of gold nano-particle arrays using two-dimensional templates from holographic lithography *Curr. Appl. Phys.* **9** 820–5
[23] Kim D, Giermann A L and Thompson C V 2009 Solid-state dewetting of patterned thin films *Appl. Phys. Lett.* **95** 251903
[24] Ye J and Thompson C V 2010 Regular pattern formation through the retraction and pinch-off of edges during sold-state dewetting of patterned single crystal films *Phys. Rev.* B **82** 193408
[25] Sundar A, Decker C J, Hughes R A and Neretina S 2012 The templated assembly of highly faceted three-dimensional gold microstructures into periodic arrays *Mater. Lett.* **76** 155–8
[26] Farzinpour P, Sundar A, Gilroy K D, Eskin Z E, Hughes R A and Neretina S 2012 Dynamic templating: a large area processing route for the assembly of periodic arrays of sub-micrometer and nanoscale structures, submitted
[27] Giermann A L and Thompson C V 2011 Requirements for graphoepitaxial alignment through solid-state dewetting of Au films *J. Appl. Phys.* **109** 083520
[28] Yang S, Xu F, Ostendorp S, Wilde G, Zhao H and Lei Y 2011 Template-confined dewetting process to surface nanopatterns: fabrication, structural tunability, and structure-related properties *Adv. Funct. Mater.* **21** 2446
[29] Hong S, Kang T, Choi D, Choi Y and Lee L P 2012 Self-assembled three-dimensional nanocrown array *ACS Nano* **6** 5803–8
[30] Beszeda I, Gontier-Moya E G and Imre A W 2005 Surface Ostwald-ripening and evaporation of gold beaded films on sapphire *Appl. Phys.* A **81** 673–7
[31] Li B Q and Zuo J M 2003 Self assembly of epitaxial Ag nanoclusters on H-terminated Si(111) surfaces *J. Appl. Phys.* **94** 743–8
[32] Basu J, Carter C B, Divakar R, Mukherjee B and Ravishankar N 2009 Nanopatterning by solid-state dewetting on reconstructed ceramic surfaces *Appl. Phys. Lett.* **94** 171114
[33] Sundar A, Hughes R A, Farzinpour P, Gilroy K D, Devenyi G A, Preston J S and Neretina S 2012 Manipulating the size distribution of supported gold nanostructures *Appl. Phys. Lett.* **100** 013111
[34] Rasband W S 1997–2012 *ImageJ US National Institutes of Health* Bethesda, MD http:rsb.info.nih.gov/ij/

[35] Malyi O and Rabkin E 2012 The effect of evaporation on the size and shape evolution of faceted gold nanoparticles on sapphire *Acta Mater.* **60** 261–8
[36] Tyson W R 1977 Surface free energy estimates of solid metals: estimation from liquid surface tension measurements *Surf. Sci.* **62** 267–76
[37] Copel M, Reuter M C, Kaxiras E and Tromp R M 1989 Surfactants in epitaxial-growth *Phys. Rev. Lett.* **63** 632–5
[38] de Miguel J J and Miranda R 2002 Atomic aspects in the epitaxial growth of metallic superlattices and nanostructures *J. Phys.: Condens. Matter* **14** R1063–97
[39] Vandervegt H A, van Pinxteren H M, Lohmeier M, Vlieg E and Thorton J M C 1992 Surfactant-induced layer-by-layer growth of Ag on Ag(111) *Phys. Rev. Lett.* **68** 3335–8
[40] Park K H, Ha J S, Park S J and Lee E H 1997 Ag growth on Si(111) with an Sb surfactant investigated by scanning tunneling microscopy *Surf. Sci.* **380** 258–63
[41] Oppo S, Fiorentini V and Scheffler M 1993 Theory of adsorption and surfactant effect of Sb on Ag(111) *Phys. Rev. Lett.* **71** 2437–40
[42] Protsenko P, Garandet J-P, Voytovych R and Eustathopoulos N 2010 Thermodynamics and kinetics of dissolutive wetting of Si by liquid Cu *Acta Mater.* **58** 6565–74
[43] Kozlova O, Voytovvych R, Prosenko P and Eustathopoulos N 2010 Non-reactive dissolutive wetting of Ag–Cu alloys on Cu substrates *J. Mater. Sci.* **45** 2099–105
[44] Webb E B III, Grest G S, Heine D R and Hoyt J J 2005 Dissolutive wetting of Ag on Cu: a molecular dynamics simulation study *Acta Mater.* **53** 3163–77